

**THE BLOCKING PROPERTIES OF STYRENE-STYRENE SULFONIC ACID
SODIUM SALT COPOLYMER AS A NANODISPERSING AGENT
IN WATER-BASED DRILLING FLUIDS**

Junwei Fang^{1,2}, Li Fan³, Jun Zhang^{1,2}, Mingyi Deng³, Gang Xie^{3*}

Nanoplugging materials are used in drilling fluid systems to seal nanopores and cracks in the shale formation, which is a focus for developing shale gas. In this work, nanoparticles of the St-NaSS copolymer were synthesized by emulsion polymerization of styrene and styrene sulfonic acid sodium salt as monomers. The St-NaSS copolymer was characterized by FT-IR, TGA, and light scattering phase analysis. The results show that the grain size of the St-NaSS copolymer nanoparticles ranges from 37 to 50 nm, and the average diameter is about 43.2 nm. The decomposition temperature of the St-NaSS copolymer is 410.7°C, indicating that the material has good temperature resistance. The St-NaSS nanoparticles have little effect on the rheological properties of the water-based drilling fluid. The plugging performance of the St-NaSS nanoparticles was evaluated by the mud cake simulation method. The permeability of the mud cake is $3.32 \times 10^{-5} \mu\text{m}^2$, which is close in value to that of the shale. When the drilling fluid contains 0.5 wt.% of St-NaSS nanoparticles, the plugging rate is 88.93%. The plugging rate of the mud cake increases with increase in the concentration of the St-NaSS nanoparticles. When the amount of the St-NaSS nanoparticles is 1.0%, the plugging

¹Petroleum Engineering Technology Research Institute, Northwest Oilfield Company, Sinopec, Urumqi, Xinjiang, 830011, China. ²Key Laboratory of Enhanced Recovery for Fracture-Cave Oil Reservoir, Sinopec, Urumqi, Xinjiang, 830011, China. ³State Key Laboratory of Oil and Gas Reservoir Geology and Exploitation of Southwest Petroleum University, Chengdu, 610500, China. *Corresponding author: Gang Xie. E-mail: 201899010129@swpu.edu.cn.* Translated from *Khimiya i Tekhnologiya Topliv i Masel*, No. 1, pp. 62-67, January – February, 2021.

effect of the drilling fluid is excellent. Therefore, St-NaSS copolymer nanoparticles can be successfully applied as a plugging agent to provide borehole stability in the shale formation.

Keywords: *nanoplugging agent; styrene-styrene sulfonic acid sodium salt copolymer; mud cake; plugging performance.*

1 INTRODUCTION

Shale gas as a commercial green and clean energy resource has been widely developed around the world [1, 2]. Shale gas resource has great potential, and the exploration and development of shale gas have become a research hotspot [3-5]. During shale gas drilling, the shale formation tends to hydrate, causing downhole complexities such as wellbore collapse, tight wells, and stuck pipes. Most horizontal shale gas wells use oil-based drilling fluids, which can provide satisfactory borehole wall stability and excellent lubrication performance [6-8]. However, oil-based drilling fluids can still cause borehole wall instability due to the hydraulic fracturing effect. When the oil molecules permeate through the microfractures in the shale formation, the combined effect of positive differential pressure and capillary force leads to the opening of new microcracks, reduces the friction of the joint surface, and significantly decreases the well circumferential stress. The more widespread use of oil-based drilling fluids is restricted by the high cost, severe environmental pollution, and strict environmental protection regulations [9, 10]. Therefore, the development of water-based drilling fluids with properties compatible with those of oil-based drilling fluids is the trend of current drilling fluid technology. Due to the development of pores and microfractures in shale formations, the hydraulic capping effect or the hydration expansion of clay minerals does not occur as long as the fluid can be prevented from entering the microfractures in the formation. Therefore, nanosealing materials are used in the drilling fluid system to seal the cracks and pores in the formation [11].

The particle size of commonly used plugging agents, such as fine calcium carbonate, bitumen, and walnut shell powder, is larger than the diameter of nanoscale pores in the shale reservoirs. As the size of microfractures and pores in shale ranges from 1 to 100 nm, the conventional plugging agents cannot effectively seal the fractures in low permeability shale reservoirs in the process of shale gas drilling. To provide effective sealing, the plugging material should contain particles of the nanoscale size. Recently, various types of materials such as nano-silica [12], nanographene [13], cellulose nanoparticles [14], carbon nanotubes [15], and hyperbranched polymers [16] have been used in the drilling fluids. Due to the nanoscale effect, agglomeration occurs easily in the nanoscale material, making it difficult to maintain nanoscale dimensions in the solution. Most inorganic nanoparticles cannot maintain long-time suspension stability in the drilling fluid system. The cationic polymer particles are prone to electrostatic interaction with the negatively charged clay particles in the solution, which results in agglomeration. In the case of anion polymer particles, the polymer nanoparticles can maintain long-time suspension stability due to electrostatic repulsion interaction between anion polymer particles and negatively charged clay particles.

In this work, the anion core-shell copolymer was synthesized by emulsion polymerization of the styrene-styrene sulfonic acid sodium salt monomers. The parameters of the copolymer were studied by the methods of Fourier transform infrared spectroscopy (FT-IR), particle size analysis, thermogravimetric analysis, and scanning electron microscopy (SEM). The plugging performance of anion core-shell copolymer as a nanoscale plugging agent was evaluated by the core simulation test.

2 MATERIALS AND METHODS

2.1 MATERIALS

Styrene, sodium styrene sulfonate, potassium peroxydisulfate, and sodium carbonate were purchased from J&K Scientific Ltd. Bentonite was obtained from Xinjiang Xiazijie. Industrial grade sulfonated lignite, sulfonated phenol-formaldehyde resin, sodium carboxymethyl cellulose, lignite sodium humate, and barite were obtained from a commercial corporation.

2.2 METHODS

The parameters of the anion core-shell copolymer were characterized by a Fourier transform infrared spectrometer (FTIR, Nicolet 6700, Thermo Scientific). The particle size analysis was carried out in Brookhaven ZetaPALS. The microstructure of the core-shell copolymer was observed using a scanning electron microscope (Quanta 450, FEI, United States). Thermogravimetric analysis (TGA/DSC1, Mettler, Switzerland) was used to measure the thermal stability with a heating rate of 15°C/min in the temperature range from 30 to 300°C. The rheological properties of water-based drilling fluids were measured by a ZNND6 rotating viscometer, manufactured by Qingdao Jiaonan Tongchun Machinery Petroleum Instrument Ltd., China.

2.3 FLUID PREPARATION AND THERMAL AGING TESTS

The formulation of the basic drilling fluid was 100 g water + 5% Na + Mt + 0.5% Na²CO³ + 0.8% carboxymethylcellulose sodium + 3% lignite sodium humate + 10% barite. The percentages of Na + Mt, carboxymethylcellulose sodium, lignite sodium humate, and barite were based on the dosage of water. The resulting basic drilling fluid was used to evaluate the rheological properties of inhibitors.

2.4 RHEOLOGICAL PARAMETERS EVALUATION

The rheological parameters such as apparent viscosity (AV), plastic viscosity (PV), and yield point (YP) were calculated from the rheometer readings in the range from 600 to 300 rpm using the following formulas [17]:

$$\text{Apparent viscosity (AV)} = \Delta\tau / \dot{\gamma} \quad (\text{mPa}\cdot\text{s}), \quad (1)$$

$$\text{Plastic viscosity (PV)} = \Delta\tau_{600} - \Delta\tau_{300} \quad (\text{mPa}\cdot\text{s}), \quad (2)$$

$$\text{Yield point (YP)} = (\Delta\tau_{300} - \text{PV}) / 2 \quad (\text{Pa}). \quad (3)$$

2.5 PLUGGING CAPACITY EVALUATION

2.5.1 Preparation of mud cake

A 10-g portion of bentonite and 0.5 g of sodium carbonate were slowly added to 100 mL of boiling water and the whole stirred vigorously for 4 h. Then 5 g of sulfonated lignite was added to the mixture and the whole stirred vigorously for 1 h. Then 5 g of sulfonated phenol-formaldehyde resin was added to the mixture and the whole stirred vigorously for 1 h. Finally, 100 g of barite was added to the mixture and the whole stirred vigorously for 1 h. The resulting standard mud was set aside for 24 h.

Before measuring the filtration volume, the resulting standard mud was stirred vigorously for 0.5 h and then placed in the HTHP filter device. The filtration volume was measured at 105°C and 3.5 MPa for 30 min, and the initial and final filtration volumes were recorded. The fluid was poured out, and the mud cake was washed

with distilled water. Distilled water was slowly injected into the HTHP filter press along the inner wall, and the filtration volume of the distilled water was measured at 105°C and 3.5 MPa. Data was recorded for 30 min with a 5-min step. The mud cake was then used for the evaluation of the plugging performance of the nanomaterial.

2.5.2 Evaluation of mud cake

The mud cake permeability was evaluated using the drilling fluid filtrate. The plugging performance of the St-NaSS material was evaluated by adding the St-NaSS nanoparticles to the filtrate. The permeability of the mud cake was calculated as

$$K = \frac{h\mu Q_t}{A\Delta P} \quad (4)$$

where K is the permeability of the mud cake, $10^{-5} \mu\text{m}^2$; A is the cross-sectional area of the mud cake, cm^2 ; ΔP is the differential pressure, MPa; h is the mud cake thickness, cm; μ is the viscosity of the solution containing St-NaSS nanoparticles, $\text{mPa}\cdot\text{s}$; and Q_t is the average flow rate, $\text{cm}^3\cdot\text{s}^{-1}$.

The plugging rate of the mud cake was calculated as [16]

$$W = \frac{(K_1 - K_2)}{K_1} \times 100\% \quad (5)$$

where W is the plugging rate; K_1 is the mud cake permeability to water without PMMA-St nanoparticles; and K_2 is the mud cake permeability to the solution containing different concentrations of the St-NaSS nanoparticles.

2.6 SYNTHESIS OF STYRENE-STYRENE SULFONIC ACID SODIUM SALT COPOLYMER

The measured amounts of styrene (20.8 g) and potassium peroxymonosulfate (0.2 g) were dissolved in deionized water (50 mL) in nitrogen atmosphere and stirred vigorously for 3 h at 75°C. A solution of styrene sulfonic acid sodium salt (41.2 g) and potassium peroxymonosulfate (0.2 g) in deionized water (50 mL) was added to the styrene solution and the whole stirred vigorously for 18 h at 75°C. The crude samples were isolated by filtration, washed, and dried by suction [18, 19] to obtain styrene-sodium styrene

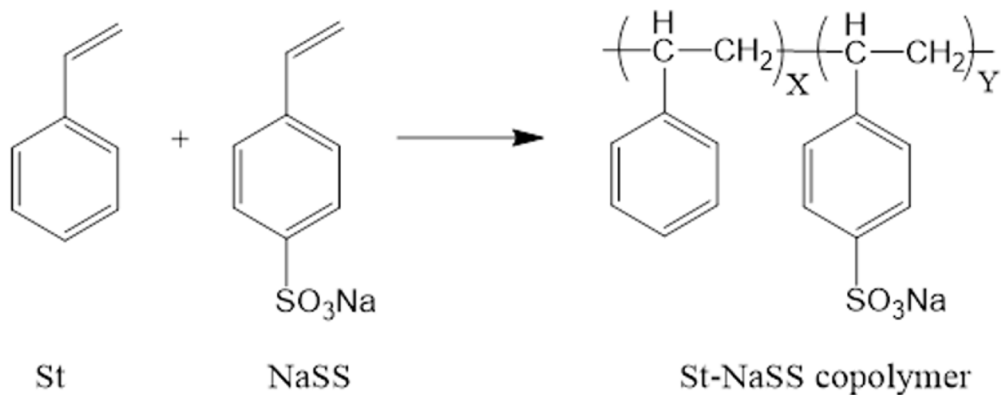


Fig.1. Copolymerization reaction of styrene and sodium styrene sulfonate.

sulfonate (St-NaSS) copolymer nanoparticles. The core-shell structure of the copolymer consists of styrene as the core and sodium styrene sulfonate as the shell. The reaction of copolymerization of styrene and sodium styrene sulfonate is shown in Fig. 1.

3 RESULTS AND DISCUSSION

3.1 FT-IR

The FT-IR spectrum of St-NaSS copolymer is shown in Fig. 2. The peak at 3430 cm^{-1} is attributable to the O-H stretch of the sulfonic acid group ($-\text{SO}_3\text{H}$). The peak at 2920 cm^{-1} is attributable to the $-\text{CH}_2$ and $-\text{CH}_3$ stretch. The peak at 1660 cm^{-1} is the absorption peak for 1,4-disubstituted benzene resulted from sodium styrene sulfonate. The peaks at 1600 , 1590 , and 1500 cm^{-1} were the skeleton vibration peaks of the

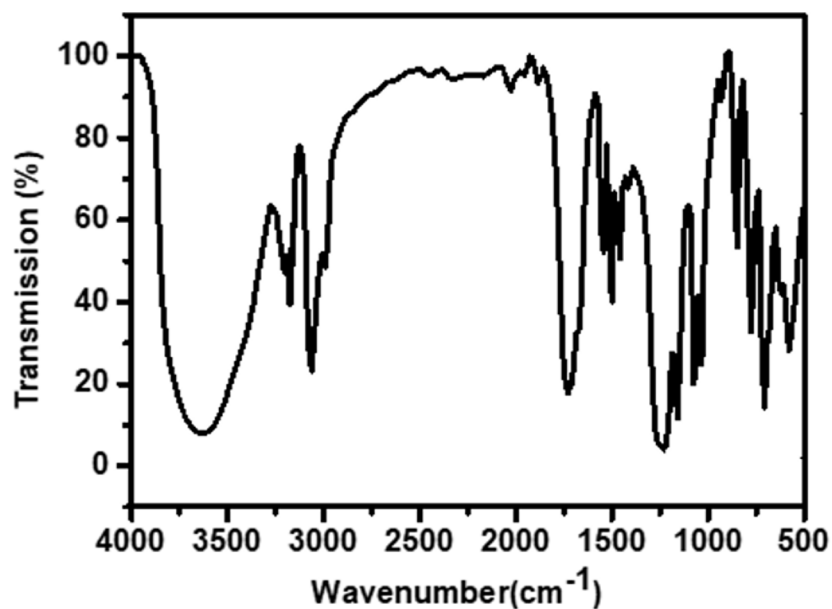


Fig.2. FT-IR spectrum of St-NaSS copolymer.

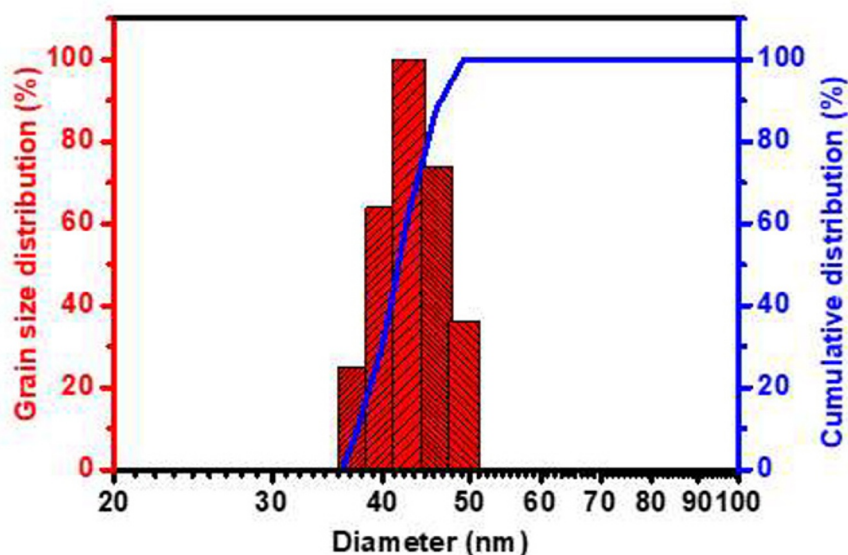


Fig.3. The grain size distribution and cumulative distribution of the St-NaSS copolymer nanoparticles.

benzene ring. The peaks at 1190 and 1040 cm^{-1} are attributable to the characteristic absorption of the S=O bond in the sulfonic acid group. The peaks at 756 and 700 cm^{-1} are the vibration characteristic absorption peaks of the mono-substituted benzene ring [20]. The results show that the synthetic copolymer contains a sulfonic acid group, benzene ring, methyl, and methylene, indicating that St-NaSS copolymer was successfully synthesized and the structure ideally corresponded to the designed structure.

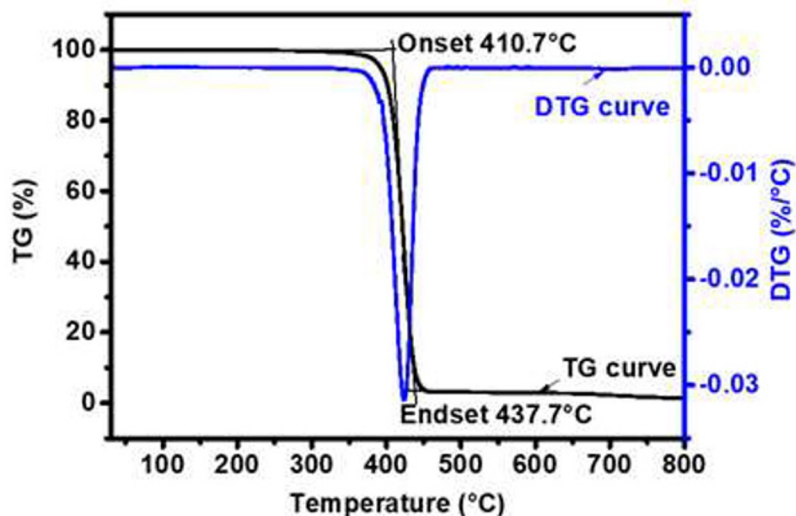


Fig.4. Thermogravimetric analysis of St-NaSS nanoparticles.

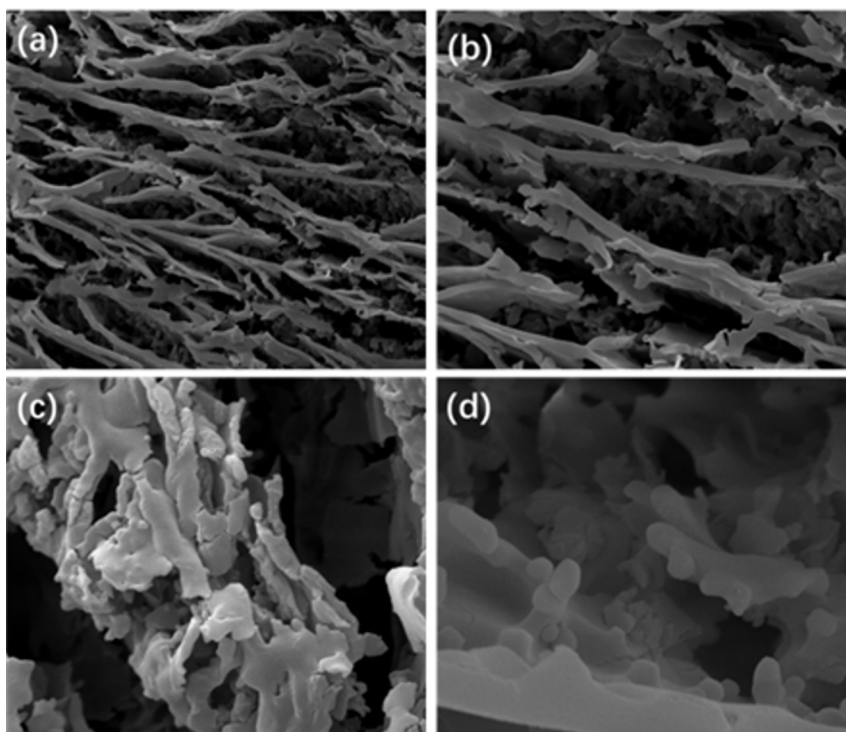


Fig. 5. SEM images of the St-NaSS nanoparticles at different magnification. a) 1000 \times , b) 2000 \times , c) 5000 \times , and d) 10000 \times .

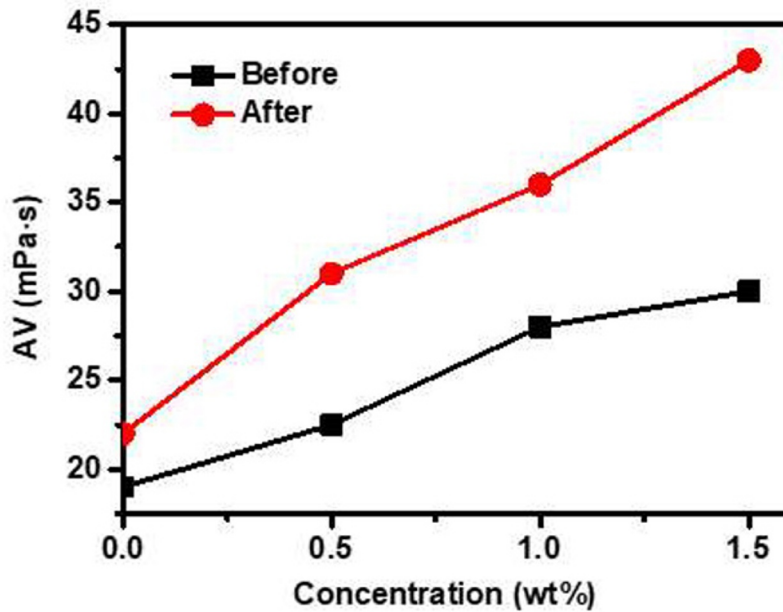


Fig. 6. AV data of drilling fluids with different St-NaSS nanoparticle concentrations (before and after hot rolling tests at 105°C for 16 h).

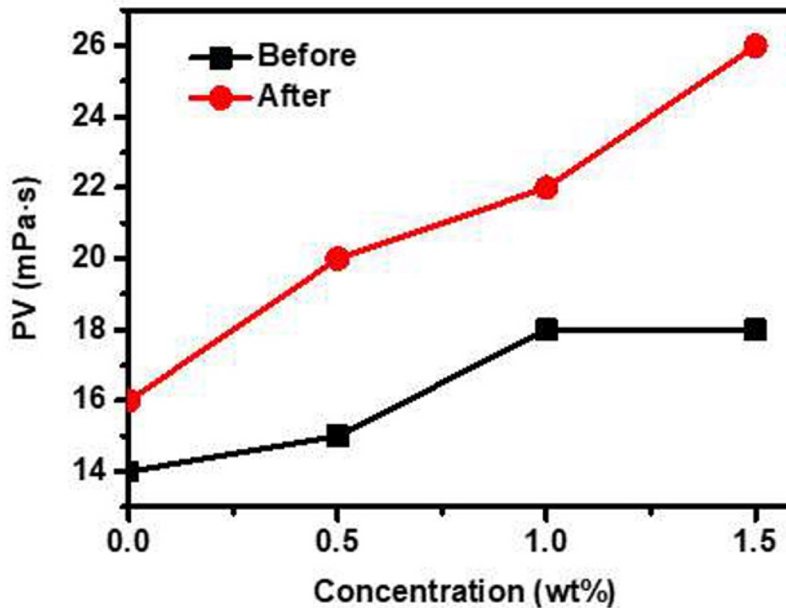


Fig. 7. PV data of drilling fluids with different St-NaSS nanoparticle concentrations (before and after hot rolling tests at 105°C for 16 h).

3.2 GRAIN SIZE DISTRIBUTION

The particle size of St-NaSS copolymer was measured by a ZetaPALS, a laser particle size instrument from Brookhaven Instruments; the results are shown in Fig. 3. Figure 3 shows that the grain size distribution of the St-NaSS copolymer is relatively narrow. The grain size mostly ranges from 37 to 50 nm, and the average grain diameter is 43.2 nm. It can be seen that the grain size of St-NaSS nanoparticles is smaller than the size of pores and fractures in shale. The St-NaSS nanoparticles are smaller than 100 nm and can effectively block the nanoscale pores and cracks in shale. Moreover, the grain size of St-NaSS nanoparticles indicates that the St-NaSS copolymer material can be effectively used in water-based drilling fluids.

3.3 THERMOSTABILITY OF ST-NASS NANOPARTICLES

The thermogravimetric curve of St-NaSS nanoparticles is shown in Fig. 4. The onset temperature is 410.7°C, which indicates that the St-NaSS nanoparticles do not undergo thermal degradation at temperatures below 410.7°C. The St-NaSS nanoparticles start to decompose with increase in temperature owing to the polymer decomposition. When the temperature rises from 410.7°C to 437.7°C, the weight of the St-NaSS nanoparticles decreases by 90.24-90.56%. The results indicate that the St-NaSS copolymer has good temperature resistance and can be used in high-temperature deep-well drilling processes.

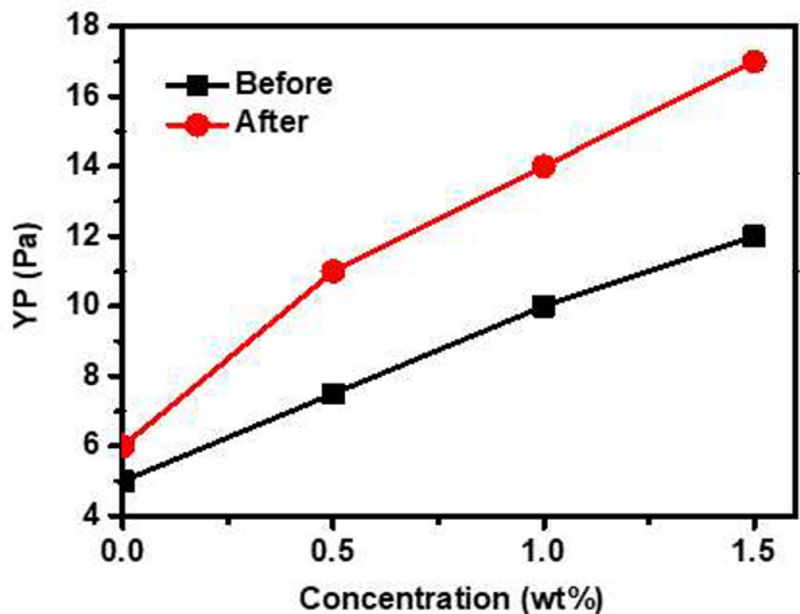


Fig. 8. YP data of drilling fluids with different St-NaSS nanoparticle concentrations (before and after hot rolling tests at 105°C for 16 h).

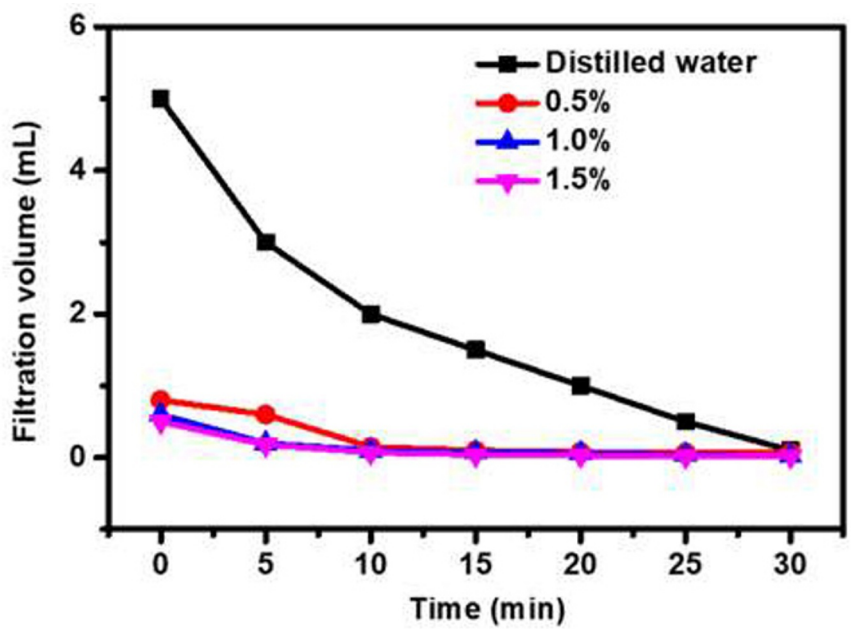


Fig. 9. The filtration volume of mud cake with different concentrations of St-NaSS nanoparticles at different times.

3.4 SEM

Figure 5 shows the SEM images of the St-NaSS nanoparticles at different magnifications. The results show that the St-NaSS copolymer structure consists of multiple foliated lamellae. However, the particle size results indicate that the shape of the St-NaSS nanoparticles is spherical. The reason is that the SEM images present the original structural appearance of the St-NaSS nanoparticles, while the particle size analysis measures the dynamic particle size of the St-NaSS particles containing the hydrated shell of the St-NaSS copolymer. The SEM images of St-NaSS copolymer prove the dense structure of the particles.

3.5. RHEOLOGICAL AND FILTRATE PROPERTIES OF WATER-BASED DRILLING FLUID

The rheological properties (AV, PV, and YP) of the basic drilling fluid containing different concentrations of the St-NaSS nanoparticles are shown in Figs. 6, 7, and 8, respectively. When the St-NaSS nanoparticles are added to the basic drilling fluid, the rheological parameters (AV, PV, and YP) increase both before and after hot rolling treatment at 105°C for 16 h. The reason is that the addition of the St-NaSS nanoparticles causes aggregation of clay particles in the drilling fluid system and increases the structural viscosity of the fluid. However, with increase in the particle concentration, the rheological parameters before and after the hot rolling test increase insignificantly. This shows that the St-NaSS nanoparticle concentration has little effect on the rheological properties of water-based drilling fluids. The results show that the optimal amount of the St-NaSS nanoparticles is 1.0 wt %.

3.6 PLUGGING PERFORMANCE OF ST-NASS NANOPARTICLES

To simulate the formation core, mud cake evaluation tests were carried out. The mud cake tests have the advantages of low cost and good reproducibility. The filtration volume of different concentrations of the St-NaSS copolymer at different times is shown in Fig. 9. The results show that compared with the filtration loss volume of the mud cake containing filtrate, the filtration loss volume of the mud cake containing the St-NaSS nanoparticles is significantly reduced. The filtration volume decreases with increase

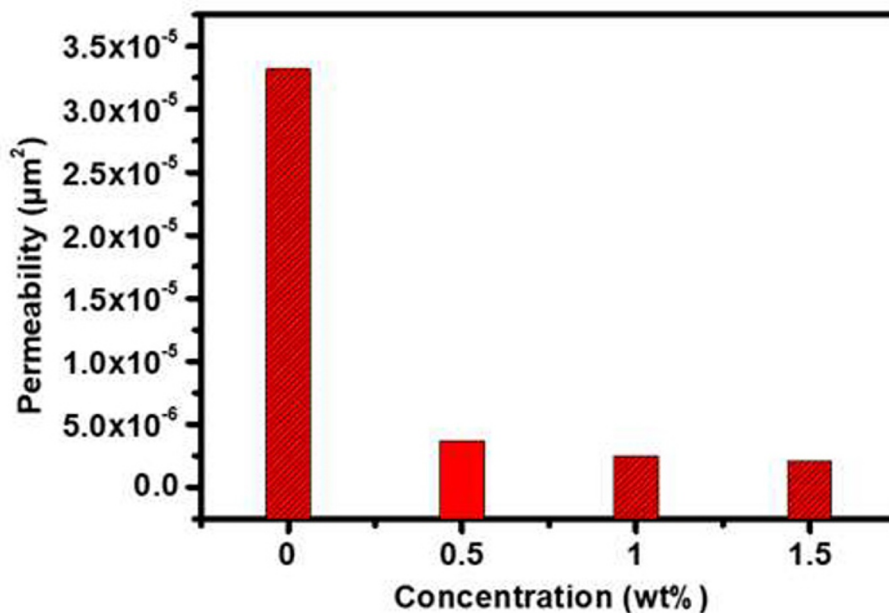


Fig.10. The permeability of mud cake with different concentration of St-NaSS nanoparticles.

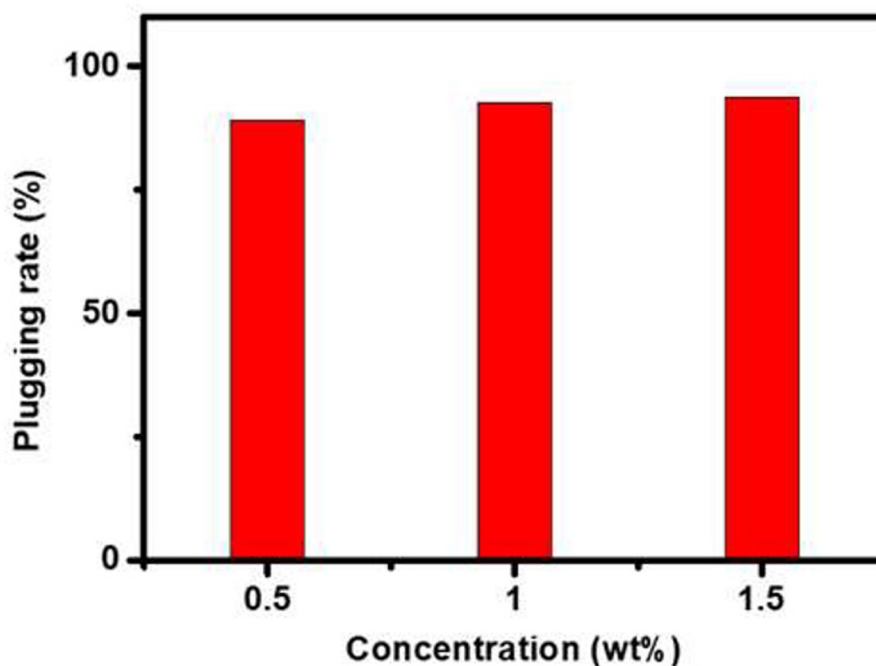


Fig.11. The plugging rate of St-NaSS nanoparticles of different concentrations.

in the concentration of the St-NaSS nanoparticles. The permeability of the mud cake calculated from Eq. (4) is $3.32 \times 10^{-5} \mu\text{m}^2$, which is close to the permeability of shale, as shown in Fig. 10. The results indicate that the mud cake test can successfully simulate the plugging performance of the St-NaSS copolymer. Compared to the permeability of mud cake with filtrate, the permeability of the mud cake containing the St-NaSS nanoparticles decreases significantly. The permeability decreases with increase in the St-NaSS nanoparticle concentration. As shown in Fig. 11, when the St-NaSS concentration is 0.5%, the plugging rate is 88.93%. When the dosage of the St-NaSS nanoparticles is 1.0% and 1.5%, the plugging rate is 92.56% and 93.83%, respectively. The plugging rate of the mud cake increases with increase in the St-NaSS concentration. When the concentration exceeds 1.0%, the plugging rate changes insignificantly. The results indicate that St-NaSS nanoparticles demonstrate excellent plugging performance when the dosage is 1.0 wt %. The results show that the optimal St-NaSS concentration is 1.0%.

The St-NaSS nanoparticles contain multiple negatively charged sulfonic acid groups, which can form a thick hydration layer and prevent particle aggregation, therefore maintaining suspension stability and plugging performance of the copolymer in the mud cake.

4 CONCLUSIONS

The St-NaSS nanoparticles were synthesized by emulsion polymerization of styrene and styrene sulfonic acid sodium salt monomers. The St-NaSS material was characterized by FT-IR, TGA, and phase analysis by the light absorption method. The grain size of the St-NaSS nanoparticles ranges from 40 to 80 nm, and the average diameter is about 45.9 nm. The grain size of the St-NaSS nanoparticles is smaller than 100 nm, so the particles can effectively block nanoscale pores and cracks in the shale formation. The St-NaSS nanoparticles have good temperature resistance, and the decomposition temperature is higher than 410.7°C.

The shale formation parameters are simulated by the low-permeability mud cake method. When the water-based drilling fluid contains the St-NaSS nanoparticles, the permeability of the mud cake decreases sharply with increase in the St-NaSS concentration. When the St-NaSS concentration exceeds 1.0 %, the plugging capacity of the drilling fluid is excellent. Therefore, St-NaSS nanoparticles can be used as an effective nanoblocking agent to provide borehole wall stability in shale.

CONFLICT OF INTERESTS

The authors declare no conflict of interests.

ACKNOWLEDGMENTS

This work was financially supported by the China Petrochemical Co. Ltd.'s major science and technology project "Shunbei Oil and Gas Field One Area Excellent Fast Drilling Technology Research" (P18021-2)

REFERENCES

1. M. Melikoglu, "Shale gas: Analysis of its role in the global energy market," *Renew. Sustain. Energ. Rev.*, 37, 460-468 (2014).
2. C. McGlade, J. Speirs, and S. Sorrell, "Unconventional gas - a review of regional and global resource estimates," *Energy*, 55, 571-584 (2013).
3. M. Liang, H. Liang, J. Yuan, and Y. Fan, "Coalbed gas and shale gas resource prospect of Heyang-Hancheng area," *IOP Conference Series Earth and Environmental Science*, 300, 022080 (2019).
4. H. Zhang, J. T. Shi, and X. F. Li, "Optimization of shale gas reservoir evaluation and assessment of shale gas resources in the Oriente basin in Ecuador," *Pet. Sci.*, 15, 756-771 (2018).
5. G. Y. Zhai, X. L. Chen, X. H. Xia, Z. Zhou, and R.H. Yuan, "The dynamic economic evaluation method of shale gas resources," *Chin. Geol.*, 2(2), 211-217 (2019).
6. X. Wang and R. Sterling, "Stability analysis of a borehole wall during horizontal directional drilling," *Tunnel. Undergr. Space Technol.*, 22, 620-632 (2007).
7. G. Bol, S. W. Wong, C. Davidson, and D. Woodland, "Borehole stability in shales," *SPE Drill. Complet.*, 9, 87-94 (1994).
8. M. Khodja, J. P. Canselier, F. Bergaya, K. Fourar, M. Khodja, N. Cohaut, and A. Benmounah, "Shale problems and water-based drilling fluid optimisation in the Hassi Messaoud Algerian oil field," *Appl. Clay Sci.*, 49, 383-393 (2010).
9. J. D. Ytrehus, M. A. Taghipour, A. Golchin, A. Saasen, and B. Prakash, "The effect of different drilling fluids on mechanical friction," *J. Energy Resour. Technol.*, 139(3), 502-508 (2017).
10. S. Ullah and N. R. Dhar, "Effects of vegetable oil based cutting fluid in machining kevlar composite material," *Am. J. Mech. Eng.*, 6(2), 54-60 (2018).
11. M.K. Chaudhury, "Spread the word about nanofluids," *Nature*, 423, 131-132 (2003).
12. J. Cai, M. E. Chenevert, M. M. Sharma, and J. E. Friedheim, "Decreasing water invasion into Atoka shale using nonmodified silica nanoparticles," *SPE Drill. Complet.*, 27, 103-112 (2012).
13. D. V. Kosynkin, G. Ceriotti, K. C. Wilson, J. R. Lomeda, J. T. Scorsone, A. D. Patel, J. E. Friedheim, and J. M. Tour, "Graphene oxide as a high-performance fluid-loss-control additive in water-based drilling fluids," *ACS Appl. Mater. Interfaces*, 4(1), 222-227 (2012).

14. M. C. Li, Q. Wu, K. Song, Y. Qing, and Y. Wu, "Cellulose nanoparticles as modifiers for rheology and fluid loss in bentonite water-based fluids," *ACS Appl. Mater. Interfaces*, 7, 5006-5016 (2015).
15. L. Ma, Y. He, P. Luo, L. Zhang, and Y. Yu, "Automatic dispersion, long-term stability of multi-walled carbon nanotubes in high concentration electrolytes," *J. Nanopart. Res.*, 20(2), 45-57 (2018).
16. G. Xie, P. Luo, M. Deng, Z. Wang, and R. Gong, "Hyperbranched polyamine as nano-plugging agent used in water-based drilling fluid," *Nanosci. Nanotechnol. Lett.*, 9, 310-315 (2017).
17. Y. An, G. Jiang, Y. Ren, L. Zhang, Y. Qi, and Q. Ge, "An environmental friendly and biodegradable shale inhibitor based on chitosan quaternary ammonium salt," *J. Pet. Sci. Engin.*, 135, 253-260 (2015).
18. D. Arunbabu, Z. Sanga, K. M. Seenimeera, and T. Jana, "Emulsion copolymerization of styrene and sodium styrene sulfonate: kinetics, monomer reactivity ratios and copolymer properties," *Polym. Int.*, 58(1), 88-96 (2009).
19. J. H. Kim, M. Chainey, M. S. El-Aasser, and J. W. Vanderhoff, "Emulsifier-free emulsion copolymerization of styrene and sodium styrene sulfonate," *J. Polym. Sci. Part A: Polym. Chem.*, 30(2), 171-183 (1992).
20. D. Lin-Vien, N. B. Colthup, W. G. Fateley, and J. G. Grasselli, *The Handbook of Infrared and Raman Characteristic Frequencies of Organic Molecules*, Academic Press, New York (1991).